

Web-Based Supervised Thematic Mapping

Javier Lozano Silva, *Student Member, IEEE*, Naiara Aginako Bengoa,
Marco Quartulli, *Senior Member, IEEE*, Igor G. Olaizola, *Senior Member, IEEE*, and Ekaitz Zulueta

Abstract—We introduce a methodology for semiautomatic thematic map generation from remotely sensed Earth Observation raster image data based on user-selected examples. The methodology is based on a probabilistic k-nearest neighbor supervised classification algorithm. Efficient operation is attained by exploiting data structures for high-dimensional indexing. The methodology is integrated in a Web-mapping server that is coupled to an HTML supervision interface that supports interactive navigation as well as model training and tuning. Quantitative classification quality and performance measurements are extracted for real optical data with 0.25 m resolution on a highly diverse training area.

Index Terms—Remote sensing, thematic mapping, Web-based mapping systems.

I. INTRODUCTION

EARTH Observation (EO) data mining systems are the subject of significant research and development efforts [1]. Petabyte-scale raster data archive volumes are growing at rates of about 10 GB per day and about 95% of their contents have never been accessed by a human observer [2]. Metadata search needs to be complemented by efficient content-based mining tools, for instance, to provide large-scale thematic mapping capabilities and similarity search based on user examples. This implies the development of new strategies and algorithms that are able to characterize and search required detailed objects/concepts. A basis for such tools is represented by semantic labeling algorithms that build upon supervised classification machine learning methods.

Such systems imply a potential expansion of the practice EO data analysis and exploitation from remote-sensing scientists and technology practitioners to application domain experts in multiple sectors. Applications can be served in environmental resource management, agronomy, ecology, risk management, and transport. The resulting applicative transition represents an evolution from Web-based cartography for casual users to thematic cover map generation based on the needs specified interactively by experts of different domains. This entails a basic set of drivers for a system implementing this concept: ease of use, scalability, and effectiveness. These three drivers can be addressed by creating high-quality supervised classification systems integrating them in scalable Web-server architectures

made accessible by simple-to-use interfaces that combine a geospatial navigation and a supervision component.

For what pertains to the actual core classification algorithm, approaches to the analysis of images acquired by remote-sensing systems include object-based, pixel-based, and hybrid methods. Classical solutions for pixel-based approaches include clustering and classification. Schröder *et al.* [3] use the input provided by the user in a Bayesian learning framework for supervised classification of a currently open image and also for finding most relevant images (images with large extents of the trained class) across an archive. Costa *et al.* [4] present a supervised per-pixel classification followed by a postclassification processing with image segmentation and semantic map generalization. The results show that segmentation of high spatial resolution images and semantic map generalization can be used in an operational context to automatically produce land-cover maps. A hybrid example can be found in [5], with the use of images from QuickBird over Arizona to compare object-based and pixel-based approaches. Their study demonstrates that the object-based classifier improves significantly over classical per-pixel results. An example of combination of techniques can be found in the work developed by Maulik and Sarkar [6]. The authors propose a scalable parallel clustering algorithm of multispectral remote-sensing imagery using point symmetry-based distance. They use a K-d tree-based nearest neighbor search algorithm to compute this distance.

Visual interaction applied to remote-sensing technologies is another topic that is becoming of great interest for the scientific community. Ho *et al.* [7] introduce a framework and class library to shorten the time and effort needed to develop Web applications for visual geospatial analytics and provides a collection of geographical and information visualization representations. Keel [8] introduces an environment for the support of remote-collaborative sense-making activities. The system has computational agents that infer relationships among information items by the analysis of their spatial and temporal organization. Within this kind of work, user interaction, user friendly environments and user interface design are issues that acquire great relevance.

The present contribution has two main aspects: 1) an algorithmic one and 2) a system development one. On the algorithm side, we extend a probabilistic k-nearest neighbor classification developed in the database domain to the generation of multi-class thematic layers from user supervision. To the best of our knowledge, this is the first time that this algorithm is considered and evaluated for large-scale thematic map generation from submetric resolution remote-sensing imagery. Furthermore, we address the issue of performance in the case of large multi-dimensional datasets by introducing efficient data structures

Manuscript received September 23, 2014; revised April 09, 2015; accepted May 11, 2015. Date of publication June 16, 2015; date of current version July 20, 2015.

J. Lozano, N. Aginako, M. Quartulli, and I. G. Olaizola are with Digital Television and Multimedia Services, Vicomtech, Donostia 20009, Spain (e-mail: jlozano@vicomtech.org).

E. Zulueta is with the Department of System Engineering and Automation, EHU/UPV, VitoriaGasteiz 01006, Spain.

Color versions of one or more of the figures in this paper are available online at <http://ieeexplore.ieee.org>.

Digital Object Identifier 10.1109/JSTARS.2015.2438034

based on K-d trees. On the side of system implementation, we develop a preoperational prototype that includes a Web-based user interface and both a Web-mapping and a supervised classification server. A user interface (UI) allows domain experts to navigate large volumes of geospatial data and provide training to the machine learning components on the server. The machine learning server computes thematic layers by supervised classification based on the efficient data structures that it maintains.

This paper is organized as follows. Section II introduces theoretical concepts used in the development of the presented prototype. Section III describes system architecture, including a description of the workflow process. Section IV presents the created evaluation framework. In Section V, measured performance values are presented and analyzed. Finally, conclusion is presented.

II. METHODOLOGICAL APPROACH

Unlike [9], which considers unsupervised classification approaches, we focus on including the user in the training process. An interactive learning scheme allows a supervisor to define examples by interacting with a Web-based geo-visualization interface. Interaction events directly influence a probabilistic model of the thematic class of interest that is built on top of an indexing structure.

This supervised thematic mapping involves uncertainties in the form of noise in the data and of uncertainties in the training provided by the users. The principled management of these uncertainties requires probabilistic classification algorithms, while operational efficiency requires that such algorithms are implemented on top of efficient data structures for large N-dimensional datasets. This section presents the probabilistic k-nearest neighbor algorithm selected for the thematic mapping service, and describes its efficient implementation in terms of K-d trees.

A. Supervised Probabilistic Classification Algorithm

The specific version of the classification algorithm that we employ is closely related to the probability threshold k-nearest neighbor (T-k-PNN) in [10], which is designed to return a most probable set S from D for a given data point o_i such that

$$S|S \subseteq D \bigwedge |S| = k \text{ and } p(S) \geq T, \text{ where } T \in [0, 1].$$

In this, the qualification probability $p(S)$ of a k -subset S is computed as

$$p(S) = \sum_{o_i \in S} \int_0^{+\infty} d_i(r) \prod_{o_j \in S - \{o_i\}} D_j(r) \prod_{o_h \in D - S} (1 - D_h(r)) dr \quad (1)$$

where the distance pdf of uncertain training pixel o_i is denoted by $d_i(r)$ while its cumulative density function (cdf) is denoted by $D_i(r)$, $r \in \mathbb{R}$ being a value taken on by the absolute distance $r_i = |o_i - q|$ to the query point q , and where pdfs are estimated

TABLE I
SYMBOLS FOR (1) DESCRIBING THE PROBABILISTIC k -NEAREST NEIGHBOR SUPERVISED CLASSIFICATION ALGORITHM

Symbol	Meaning
S	Point class—image region class
D	Uncertain database—image regions to classify
k	Number of points
$p(S)$	Quantification probability of S
T	Probability threshold
o_i	Uncertain object of $D(i = 1, \dots, D)$ i —training image region
q	Query point—image region with unknown class
r_i	$ o_i - q $ Distance from current region to training
$d_i(r)$	PDF of r_i (distance Probability Density Function)
$D_i(r)$	CDF of r_i (distance Cumulative density Function) or Distance relative to ownership of the class.
$D_h(r)$	CDF of r_h (distance Cumulative Density Function) or Distance relative to the other classes

by kernel-based estimation and numerically integrated in cdfs. Table I summarizes the symbols in (1).

The merging process by (1) can be carried out based on estimating and minimizing a per-pixel distance $r_i(o_i, q)$ to the nearest training element in either the feature or the geographic space, resulting in a pure multiclass classification or in a multi-class classification with a significant segmentation component related to the spatial dimension.

The authors of the methodology [10] observe that (1) can be understood by considering that in order for S to be a query answer, the distance of any object o_h (where $o_h \notin S$) from q must be greater than that of o_i where $o_i \in S$. At distance r , the pdf that object $o_i \in S$ has the k th shortest distance from q is the product of the following factors:

- 1) the pdf that o_i has a distance of r from q , i.e., $d_i(r)$;
- 2) the probability that all objects in S other than o_i have shorter distances than r , i.e., $\prod_{o_j \in S \wedge o_j \neq o_i} D_j(r)$; and
- 3) the probability that objects in $D - S$ have longer distances than r , i.e., $\prod_{o_h \in D - S} (1 - D_h(r))$.

The integration function in (1) is essentially the product of the above three factors. By integrating this function over $(0, +\infty)$, we obtain the probability that S contains the k nearest neighbors with o_i as the k th nearest neighbor. Finally, by summing up this probability value for all objects $o_i \in S$, (1) is obtained.

B. K-d Tree-Based Implementation

The authors observe in their contribution that (1) is inefficient to evaluate, requiring as it does the computation of the distance pdf and cdf of each object, a costly numerical integration over a large range.

The exploitation of efficient data structures such as K-d trees allows the developed system to perform efficiently to the point of supporting efficient queries across a network environment.

Pixel-based approaches [3] require processing very large data volumes. In this sense, to get an efficient response to the queries, data organization is critical. In particular, nearest neighbor search can benefit from hierarchical indexing structures. K-d trees are space partitioning data structures for point organization in k-dimensional Euclidean spaces. They are based on sets of hyperplanes each perpendicular to one of the axes of the coordinate system. All nodes in the tree, including root and leaves, store a point and a space-dividing hyperplane.

To efficiently find the nearest neighbors, it is necessary to define a local search scope which is accomplished by the K-d tree. The key benefit is the reduction in the computational cost to find the nearest neighbor from $O(n)$ to $O(\log(n))$ in the average case. This significantly improves the performance when dealing with large data archives. The tree construction algorithm used is described in Maneewongvatana and Mount [11].

In the thematic layer generation process, the user selects different training regions. As we have seen, the result of this selection is modeled as a combination of random variables in a feature space with an associated pdf. This requires the use of proper kernel estimation techniques to go from training histograms obtained by selecting areas of interest to full pdf estimations.

This approach uses different generalization radius parameters, for each of the training points. The final results are obtained by operations on the generated K-d trees.

If a multiclass problem is considered, a situation in which a same pixel is classified in different classes needs to be solved by (1).

C. Implementation Details

In an actual optimized algorithm execution flow, (1) needs to be computed repeatedly for all the pixel regions to be classified. A caching mechanism based on memorized functions is used in order to avoid recomputing results, as in dynamic programming schemes. In order to reduce processing costs, the integral is computed as a quantized sum over the space of distances. The processing cost is further reduced by only computing the distances for couples that are nearby according to batched queries to a K-d tree instantiated based on feature values for user-provided supervision training areas.

D. Data Characteristics and Primitive Features

Advances in remote-sensing technology have improved in quality and quantity of the images that we have available. Until recently, the decametric resolution of this kind of images has limited observable classes to urban areas, forest, agricultural areas, bare soil areas, and water bodies. With metric resolution images, the development of new strategies and methodologies is necessary.

In this contribution, we consider data available in the Open Data Euskadi repository.¹ In this specific work, we considered multiple test sites, with a composite size of about $25\,000 \times 5000$ pixels, with a resolution corresponding to 25 cm in each

TABLE II
PRIMITIVE RADIOMETRIC AND GEOMETRIC DESCRIPTORS WITH
EXTRACTION PARAMETERS

Descriptor name	Analysis region size	Angular quantization	Reference
HSV	1×1	None	[26]
Histograms of oriented Gradients (HOG)	12×12	8	[27]
Local binary Patterns (LBP)	24×24	8	[27]
Right-angle Detector (LSD)	12×12	4	[28]
Edge density	12×12	None	[29]
Sift density	24×24	None	[28]

direction. As is typical of image acquisition systems with very high geometric resolution, the radiometric resolution of the acquired data is limited to a limited number of channels.

CBIR literature typically devotes significant efforts to the careful choice and implementation of image content descriptors [12].

The literature of image analysis includes a diverse gamut of content-based primitive feature extractors, ranging from pixel-based descriptors like color to geometrical ones such as texture [13]–[15]. The use of combinations of these features is also usual [1], [16].

Global and image-level descriptors are often complemented by local ones. While the former ones have properties desirable for the discrimination of the semantic context of the scene, the latter ones enable the characterization and recognition of specific elements of the scene. The proper composition of discrimination strategies at the semantic context and at the object level is the subject of a large corpus of research [1], [17], [18].

As indicated by state of the art results in metric resolution classification for remote-sensing applications [19], except the HSV color-based descriptor the considered primitive features are region-based: histograms of oriented gradients (HOGs), local binary patterns (LBP), a right-angle/line segment detector (LSD), edge density, and SIFT.

In [20] land cover changes of the last 40 years in the country of Mali are analyzed. Object-based feature extraction and supervised (maximum likelihood) and unsupervised (ISODATA) classification are used to this end on high resolution panchromatic and multispectral remote-sensing imagery.

A framework is presented on [21] for building extraction from visible band images. Combining supervised and unsupervised classification, accurate rooftop extraction is achieved using a Higher order Conditional Random Field.

Another framework is presented in [22], where weakly supervised learning and high-level feature learning layers are combined: SIFT descriptors are clustered by K -means and fed to deep Boltzmann machines to capture structural and spatial patterns.

In [23], the problem of learning high-level features from a limited labeled subset in a large amount of unlabeled data is addressed using semisupervised ensemble projection (SSEP). The proposed method represents an image by projecting it

¹[Online]. Available: <http://opendata.euskadi.net/>

TABLE III
CHARACTERISTICS OF THE TEST SITES USED IN THE EVALUATION

Site id	Site name	Center (Lat/Lon)	Site description	Ground cover classes
1	La Concha	43.3190, -1.9923	Bay area	Bare soil, beach, buildings, pasture, roads, sea, woodland and urban area.
2	Arratz-Errek a	43.0056, -2.4737	Mountain area	Bare soil, beach, buildings, fields, pasture, roads, scrubs, and, woodland
3	Barakaldo	43.2986, -3.0004	Industrial area	Buildings, industrial, roads, urban and water
4	Vitoria Gasteiz	42.8505, -2.6690	Mixed urban area	Buildings, roads, and urban
5	Urdaibai	43.3837, -2.6905	Estuary natural reservoir	Buildings, fields, pasture, roads, urban, water and woodland.

The five test sites represent a significant degree of contextual diversity as well as a significant number of specific ground cover classes. Rectangular bounding boxes are given as the latitude and longitude of the upper-left (north western-most) and lower-right (south eastern-most) points. Each of the five test sites has a geographical extension of $1.2 \times 1.2 \text{ km}^2$, which corresponds to about 23.6 Mpixels for each of the five input regions.

onto an ensemble of weak training (WT) sets sampled from a Gaussian approximation of multiple feature spaces.

The feature extraction approach presented in [24] consists on five steps: 1) feature extraction; 2) feature learning; 3) feature encoding; 4) feature pooling; and 5) classification. The process starts with low-level feature extraction by, e.g., SIFT. Then, a set of normalized basis functions is computed by unsupervised learning. Orthogonal matching pursuit is used for coding the basic function set. Finally, the sparse features are pooled to create the final representation to be fed to a support vector machine classifier.

In [25], an extensive evaluation of SIFT local invariant features, is conducted for the retrieval of land cover classes in high-resolution aerial imagery, with a comparison with standard features such as color and texture.

We establish an extraction process that defines a common grid among the extracted descriptors, so as to allow the subsequent data fusion procedure. This requires a spatial resolution rescaling that we implement as a nearest-neighbor interpolation for lower-resolution descriptors. Descriptions for the primitive features, with corresponding extraction parameters including region sizes, are reported in Table II.

E. Training Strategy

As in [19], the training supervision is provided to the system in terms of polygon-bounded regions manually defined over specific single-class coverage areas in the input image, see Table IV.







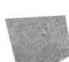





Sampling without replacement is used to extract an equal number of samples (usually in the order of the tens of thousands) for all training classes. The extracted sample sets are used for estimating pdfs for the class-specific distributions via kernel-based methods.

III. PROTOTYPE IMPLEMENTATION

While Section II describes the methodological basis of the implemented service, this section details its implementation strategy and its architecture in the form of collaborating Web-based services. Proposed system architecture is presented in Fig. 1.

As stated in the paragraphs regarding motivation in the introduction, we consider a Web-based architecture for reasons of accessibility and horizontal scalability.

TABLE IV
TRAINING PATCHES BY CLASS WITH GLOBAL TRAINING SAMPLE SIZE

Class	Training patch	Class	Training patch
Bare soil		Roads	
Beach		Scrubs	
Buildings		Sea	
Fields		Urban	
Industrial		Water	
Pasture		Woodland	

The actual pixels for training are sampled without replacement in a number of 1024 from the above global training polygons which fall within the areas identified for the class in the ground-truth map. The total size of the training sample used is therefore of $1024 \times 12 = 12\,288$ pixels, about 0.01% of the total size of about 118 MPixels for the whole pixel size of the evaluation test site set.

A. Architecture

A map sever module manages the imagery to be used by the system, both in terms of quick-looks for representation and training, and as output created thematic layer tiles. It is based on TileStache, a Python-based server application that can serve map tiles based on rendered geographic data,² Mapnik, a free toolkit for developing mapping applications³ and GDAL,⁴ a translator library for raster and vector geospatial data formats.⁴ Zoom, drag, and drop operations are available. The system generates thematic tiling at different resolution levels based on input by the user. The classification system is coupled with a tiling service for optimizing time-to-display.

The Web-server module is based on the Flask micro framework.⁵

The processing server module is in charge of image processing and classification. It computes the needed K-d trees and

²[Online]. Available: <http://tilestache.org/>

³[Online]. Available: <http://mapnik.org/>

⁴[Online]. Available: <http://www.gdal.org/>

⁵[Online]. Available: <http://flask.pocoo.org/>

performs the actual classification based on the pixels selected by the user. The processing server receives processing requests from the client module, processes them effectively and provides the resulting tiles to the Map Server. The server also provides an identification number to the client that allows to request the created thematic tiles to the map server.

The client side is a Web-based graphical user interface. This interface, with a screenshot depicted in Fig. 4, is built around an interactive map view that supports supervised training according to the semantics of the thematic class of interest. A configuration panel presents a description of the training itself and allows the user to interactively manipulate some parameters of the learned model. Interaction is managed by the event handlers of the jQuery library.⁶ Workflow process scheme is presented in Fig. 2.

B. Processing Flow

In a Web-based environment, optimizing performance issues related to data communication and memory footprint in the client is of foremost importance. In the case in which the data has a volume that allows to store it in the memory of a single server [30], [31], static K-d trees can be computed. In the case in which layer data volume hinders agile management, a dynamic strategy is needed.

The developed solution tries to be simple and effective, creating only the needed K-d trees. The created layer is limited to the available area around the visible map in the browser. This strategy requires more communication between client and server, for the server to create and process the necessary K-d trees. As the user navigates the map, the client sends to the server the information related to the visualization area.

With this information the server is able to create the K-d trees related with the navigation. Click-and-drag operations in the client move the map view port as is typical of Web-based geospatial interfaces. Events that impose an extension or a recomputation of the live area under analysis are handled by spawning new processing requests to the server. The system configuration aims at reducing these requests to a minimum, while avoiding an excessive load on the client memory.

The supervisor is free to define a semantic class based on a probabilistic composition of simpler components. each one represented by a different K-d tree instance.

An example sequence diagram is represented in Fig. 3, from client request to the creation of a thematic map in the user interface. The description of the steps is as follows:

- 1) If they are not available, the server creates tiles corresponding to the current predefined active area.
- 2) After this, K-d tree indexes from tiles are calculated for training. At this point the server is ready.
- 3) The client requests a Web page from the Web server.
- 4) The Web server receives this request and responds with an HTML Web page with the information needed to create the map.
- 5) The client requests the required map tiles from the map server.

⁶[Online]. Available: <http://www.jquery.org>

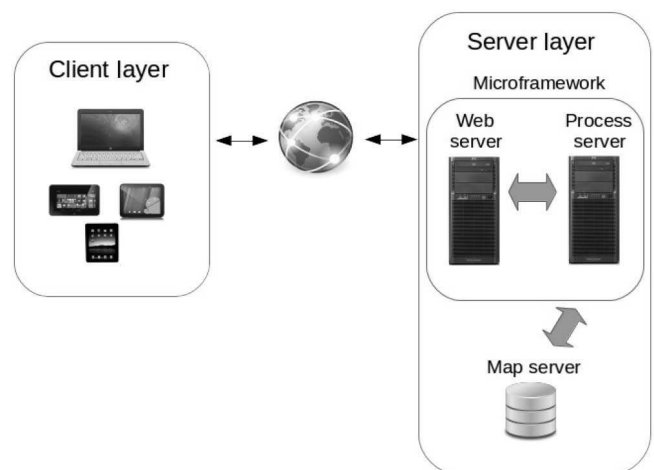


Fig. 1. Proposed system architecture in the form of different modular layers.

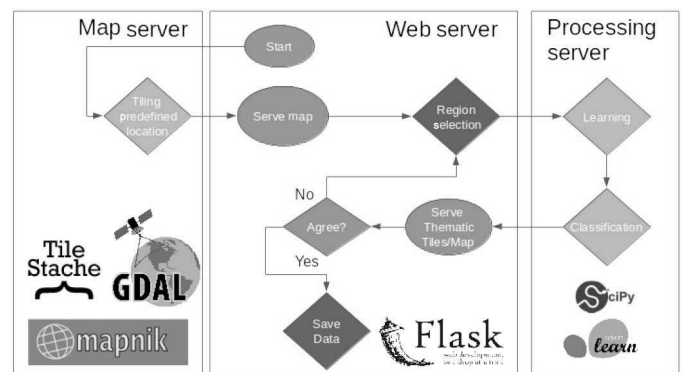


Fig. 2. Workflow process scheme for server-side operation: the map server component serves primitive feature tiles to the classification Web server that operates based on training supervision by the user. The processing server component performs the classification and serves the resulting thematic map tiles to the user for optimizing time-to-display. A complete sequence diagram including client-side operation is represented in Fig. 3.

- 6) The map server returns the needed tiles. Now the client is ready.
- 7) The user navigates around the map searching for instances of the target class.
- 8) The user selects pixels according to the semantics of the search, and can subsequently tune configuration parameters of the model.
- 9) Once the client completes the pixel selection phase, it requests the new thematic layer of the active area. Training and model configuration data are sent by AJAX asynchronous requests, allowing the application not to wait the end of response data transmission.
- 10) When the processing module receives the data, it checks if needed K-d trees are created or not, to request any required tiles to the map server.
- 11) Then needed K-d trees are processed with user selected pixel data. This process creates a tile with the nearest neighbor pixel class corresponding to the training pixels.
- 12) The tiles are stored in the map server.
- 13) Once all thematic tiles are created, an identification number is returned by the processing server to the client.

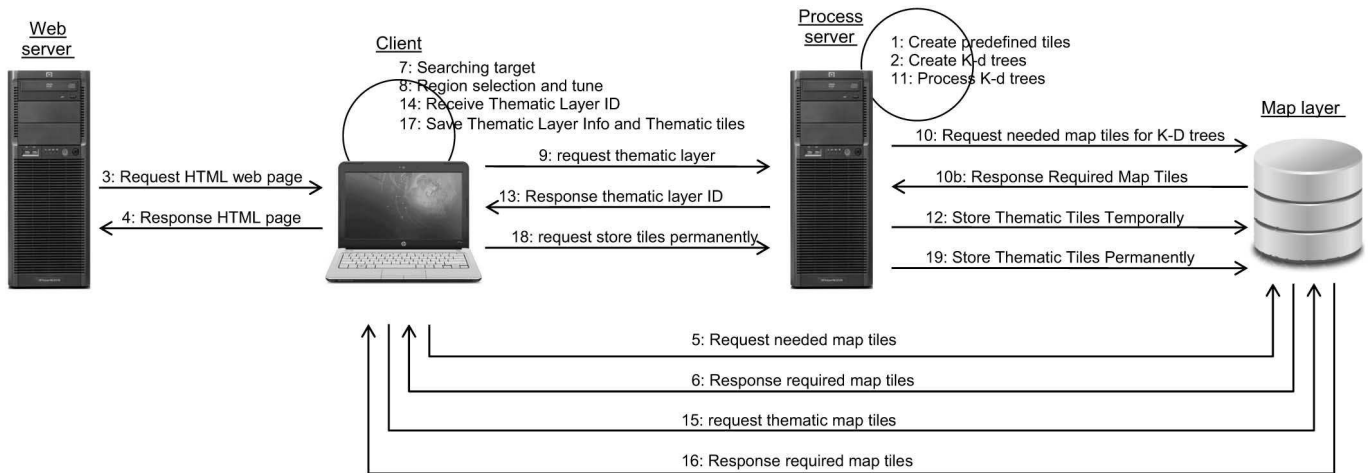


Fig. 3. Client/server thematic map creation sequence diagram.

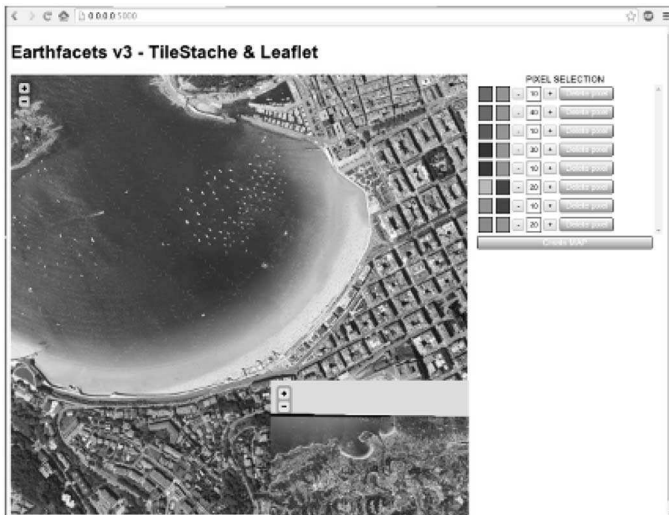


Fig. 4. User interface screenshot. An interactive map viewer supports supervised training and output presentation. A configuration panel to the right allows the user to interactively manipulate the parameters of the learned model.

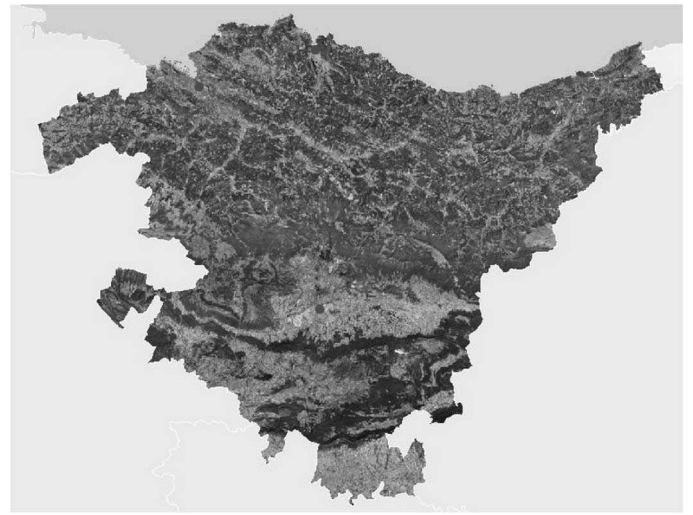


Fig. 5. Geographical location of test sites in the Basque country. From left to right, top to bottom: Bilbao industrial site, Urdaibai estuary protected area site, La Concha bay site in Donostia San Sebastian, Arratz Erreka mountain area site and Vitoria Gasteiz urban area site. These areas include the 12 different ground cover classes considered: beach, buildings, fields, industrial area, bare soil, pasture, scrubs, sea, urban area, urban roads, water. See Table III for the characteristics of the sites.

- 14) The client receives this identification number and is able to activate or deactivate the created thematic layer.
- 15) The client requests new thematic tiles.
- 16) The map server returns them.
- 17) The client is able to save the created thematic layer. It locally saves the data needed to create the thematic tiles.
- 18) The client potentially creates a save request.
- 19) The processing server receives a save request and requests to the map server to save the new tiles.

IV. EVALUATION METHODOLOGY

The end-to-end validation of the system naturally focuses on the performance evaluation of the implemented classification system, since its operation involves all subsystems in the prototype. This performance evaluation is conducted as is customary by analyzing the quality of thematic map images produced based on a well known input.

The analysis is carried out on five separate test sites located in the Basque country region Fig. 5, each with an extension of

4864 × 4864 pixels (about 1.2 km × 1.2 km each). A composition is shown in Fig. 6(a).

The sites include the 12 ground cover classes considered and corresponding to layers in reference geographical maps extracted from the Open Data Euskadi repository⁷ managed by the Basque regional government. The classes correspond to sea, water, woodland, bare soil, urban, pasture, scrubs, fields, industrial, buildings, roads, and beach.

A. Vector-Map-Based Ground-Truth Map Creation Procedure

This section describes the generation of ground-truth maps from the vector maps available in the Open Data Euskadi repository.

⁷[Online]. Available: <http://opendata.euskadi.net/>

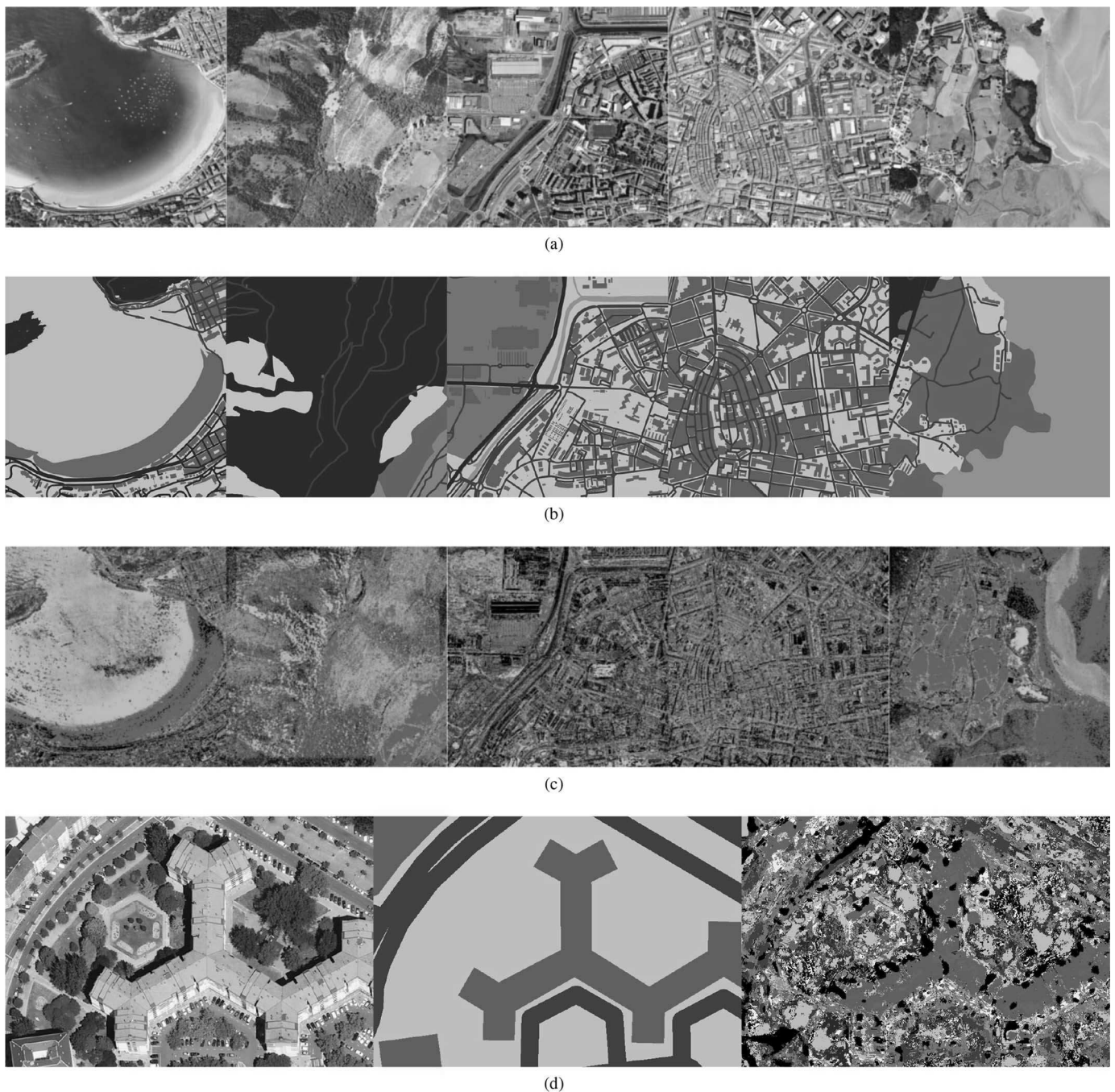


Fig. 6. Classification results. (a) Composition of the five original images of the test sites relative from left to right to La Concha bay, to the Arratz Erreka high plane, to the industrial area in the outskirts of Bilbao, to the Vitoria Gasteiz mixed urban environment and to the Urdaibai estuary protected area. (b) Corresponding composition of the five ground-truth maps based on Open Data Euskadi WMS shape files is shown in line, while (c) classification results are in line. Line (d) presents from left to right the original data, the vector-map-based ground-truth and the classification result at full resolution for the area marked with a red rectangle in the Vitoria Gasteiz ground-truth map in line (b). The classified maps are with a number of pepper-and-salt effects. In addition, some spectrally similar objects are not well identified and discriminated, such as buildings-roads-soil.

In addition to submetric resolution aerial ortho imagery of all territory, geographical information related to ground cover and usage is available in the form of vector maps. With this information, it is possible to build ground-truth models of the surface of the Basque country.

The challenge here is to complete a ground-truth model that covers all the area in the test sites to analyze, merging different categories in existing layers to obtain the most descriptive map of the area. This procedure is carried out manually: some of the

categories overlap each other and some do not appropriately cover the test sites.

The obtained ground-truth models for the test sites presented in Fig. 6(a) are shown in Fig. 6(b).

Two fundamental problems arise with the significance of the available ground truth with respect to the available imagery: a temporal and a spatial one.

A first issue is the temporal date of reference for the maps. In general, cover maps do not correspond in this respect to the

aerial imagery. A clear example of this is visible in the low tide image of the river mouth in the Urdaibai estuary site, which is represented as fully flooded in the maps.

A second issue is that the level of detail of vector data maps does not typically match that of aerial imagery with 25 cm pixel spacing, which is bound to have impacts in the performance measures. If Fig. 6(a) and (b) are compared, it is easy to detect some differences: most of the green areas in the city areas are not represented in the maps, different kinds of vegetation can be seen in the imagery that are fused in the Arratz Erreka site vector maps under the same label.

To overcome these limitations, in addition to the vector map-derived ground truth, the production of a further pixel-level, image interpretation-based ground-truth model is considered, to be able to compare obtained results with more detail.

B. Pixel-Level, Image Interpretation-Based Ground-Truth Map Creation Procedure

The definition of a multiple-class pixel-level ground-truth map based on the interpretation of submetric resolution imagery represents a significant challenge. A combination of specific training, semiautomatic tools, and careful inspection of the results are important components. A very good knowledge of and accessibility to the chosen test area are needed.

An area for testing and validation has been defined on the La Concha bay in the city of Donostia San Sebastian, where the authors are located so that field inspections can be used whenever necessary to verify the obtained results. The bay gathers different spatial contexts in a limited extension, which makes it particularly interesting as a testing location.

A first step is the selection of a representative set of semantic classes with clear meaning. In the case of our map, the eight selected classes are beach, buildings, bare soil, pasture, roads, sea, woodland, and urban area. Although these classes only represent an approximation to the twelve classes considered in the case of the vector map-derived ground truth, we still consider the set to be significant in the sense that the classes properly represent all essential visible content in the input data, and it to be orthogonal in the sense that their semantic separation is sufficiently large as to avoid significant overlaps and uncertainties in the corresponding feature space.

A well-defined procedure needs to be set up for generating an output thematic map with these characteristics from the input data. The procedure needs to exploit semiautomatic tools to generalize and extend training input provided by a human supervisor in order to speed up the overall process. The training is provided in the form of polygons covering a significant area of a given scene object. These elementary training areas need to have a sufficient geometrical extension to be able to express significant statistical descriptors from them. These statistics are computed in terms of color content as defined and simplified by means of a vector quantization with a number of levels in the order of the hundreds. To actually perform the geometrical extension of the training polygon to the observable limits of the considered scene object, the semiautomatic tools used include an edge-based segmentation routine that is launched in conjunction with every training event.

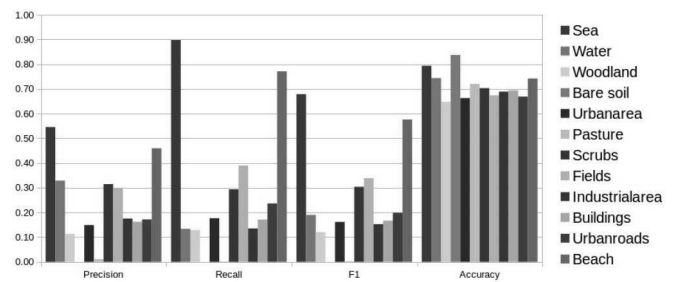


Fig. 7. Performance results for the full set of five test sites and of the 12 ground cover classes considered. Low values for classes like Beach and Water are directly related to temporal variations observable in the imagery with respect to the reference maps and to the different level of detail considered, see Fig. 4.

Once multiple tentative single-class thematic maps are defined, a procedure is needed to carefully compose them into a multiclass map. A further semiautomatic procedure is employed to highlight areas assigned to multiple classes as well as unassigned areas. The pixels in these areas are subject to an arbitration procedure in order to assign them unambiguously to a single ground-truth thematic class.

An extensive and labor-intensive supervised validation phase ensues in which the produced tentative multiclass map is inspected for dubiously labeled pixel areas.

The produced ground-truth map (Fig. 8), is currently published as open data at the URL <http://150.241.250.4:5000/earthfacets/groundtruthmap.png>. The authors hereby invite external users, specific corrections and general suggestions for improvement in the results or in the overall procedure.

C. Ground-Truth-Based Evaluation Procedure

The generated ground-truth map can be used for evaluating the performance of the system. The procedure we employ to evaluate quantitatively the obtained results can be described as follows.

- 1) Load training in the form of user selected pixel data.
- 2) The K-d trees of the tiles that compose the analysis area are calculated.
- 3) Each K-d tree is processed and a new tile is created and stored. If the training considers a multiclass problem, a new tile is created for each class.
- 4) A unique map is composed with the newly created tiles.
- 5) A confusion matrix is computed by comparing the classification output with the ground-truth map.
- 6) Performance statistics (precision, recall, F-1 measure, and accuracy, see Section V, Section IV-D are computed from the confusion matrix.
- 7) Finally, the time required for completing the process is computed.

The designed solution allows us to experiment with different user selection options and obtain quantitative results for these selections in an easy and quick way.

D. Considered Performance Measures

To evaluate system performance we select the following statistical measures of information retrieval performance:

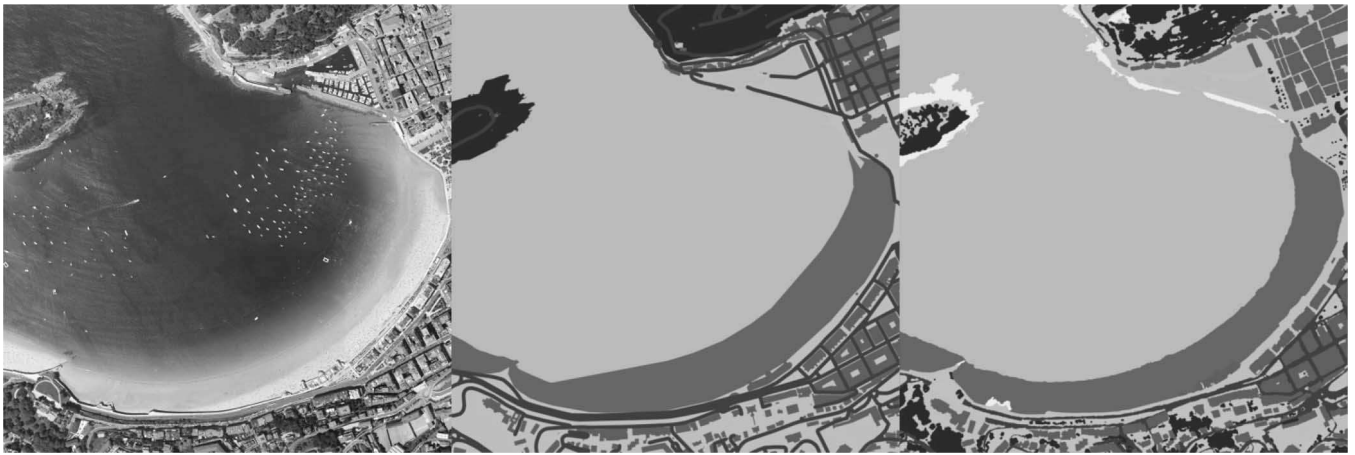


Fig. 8. From left to right: original image, pre-existing vector-map-based ground truth, manually produced pixel-level image interpretation-based ground truth for the La Concha test site. The subset of the defined ground cover classes includes eight elements from the original 12: building (purple), sea (blue), bare soil (light green), pasture (green), woodland (dark green), street (gray), urban roads (dark gray), and beach (brown). An increased level of detail is evident, particularly, in vegetated areas between buildings and near to Bare Soil areas.

TABLE V
PERFORMANCE MEASURES FOR THE COMPLETE TEST SITE COLLECTION OF FIVE AREAS BASED ON THE VECTOR MAP-BASED GROUND TRUTH WITH 12 GROUND COVER CLASSES

Performance statistics	Sea	Water	Woodland	Bare soil	Urban	Pasture	Scrubs	Fields	Industrial	Buildings	Roads	Beach
Precision	0.70	0.33	0.27	0.00	0.29	0.00	0.03	0.30	0.09	0.46	0.21	0.17
Recall	0.90	0.13	0.13	0.00	0.18	0.00	0.29	0.39	0.13	0.17	0.24	0.77
F1	0.79	0.19	0.17	0.00	0.22	0.00	0.05	0.33	0.10	0.25	0.22	0.28
Accuracy	0.83	0.70	0.58	0.83	0.57	0.86	0.80	0.68	0.72	0.66	0.61	0.74

Results are markedly inferior to the ones obtainable with reference to the manually curated image interpretation-based ground-truth map limited to the La Concha Site, due to differences in both the time reference chosen and the level of spatial detail considered.

precision, recall, F1, and accuracy [32]. The definition of the measures is as follows:

$$Precision = \frac{tp}{tp + fp} \quad (2)$$

$$Recall = \frac{tp}{tp + fn} \quad (3)$$

$$F1 = 2 \frac{Precision \cdot Recall}{Precision + Recall} \quad (4)$$

$$Accuracy = \frac{tp + tn}{tp + tn + fp + fn} \quad (5)$$

In the above, tp is the number of true positive cases, tn is the number of true negative cases, fp is the number of false positive cases, and fn is the number of false negative cases.

V. PROTOTYPE EVALUATION RESULTS

A. End to End Classifier Evaluation on Complete Test Site Set

Quantitative performance measures for the classifier on the whole set of 12 ground cover classes as evaluated on the whole test site set of five areas is described in Table V and Fig. 7.

The ground cover class with the best results is sea, with scrubs, and fields showing more limited performance and with only limited results for classes like industrial and bare soil.

An inspection of the semiautomatic ground truth based on existing vector-maps shows that the results are probably significantly affected by the characteristics of the original map data, and in particular by both the limited detail available in rural areas (hence the good results for scrubs and fields) and by the significant overgeneralization for very diverse classes such as industrial. Further effects include a mismatch in between the reference dates for the maps and the image acquisition, which shows up clearly in coastal areas subject to rapid change such as the Urdaibai estuary.

This points to the need, addressed in upcoming sections, for an evaluation with respect to both a vector-map-based ground truth and a pixel-level one.

B. Evaluation of Different Feature Approaches

Classified thematic layers per each class are merged by (1) based on estimating and minimizing a per pixel distance to the nearest training element in either the feature or the geographic space, resulting in a pure multiclass classification or in a multiclass classification with a significant segmentation component related to the spatial dimension.

An example map obtained from the N-class classification process based only on color descriptors is presented in Fig. 5(b). Typical accuracy measures are around 85% for most of the classes. A better definition of the ground coverage classes can

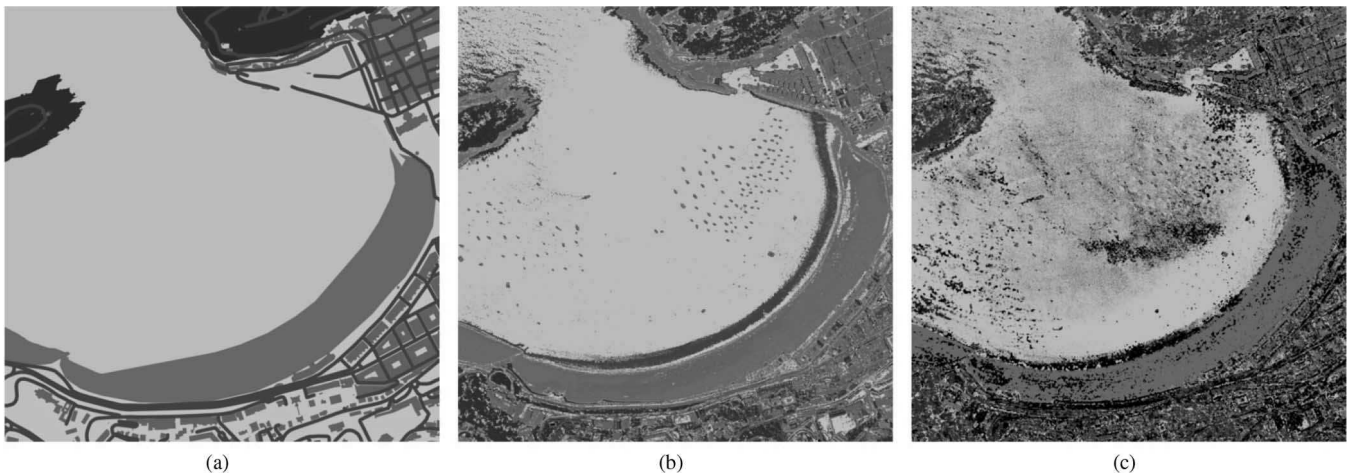


Fig. 9. (a) Ground truth based on preexisting vector map, (b) supervised classification results from color descriptors only as well as from (c) the full set of descriptors in Table II. Color encodes assigned class: building (purple), sea (blue), woodland (dark green), street (gray), urban roads (dark gray), and beach (brown). A portion of the output pixels remains unclassified (black).

be obtained by extending the training. Unlike the old town buildings which are well classified thanks their tiled roofs, the newer building area is characterized by lesser performance due to the mixed pattern of the roofs. Class street is another case for which the diversity of the patterns implies that a good characterization is more difficult to obtain.

The corresponding map obtained by considering all descriptors jointly including all the region-based ones as per Table II is in Fig. 5(b) and Fig. 10. The relative quality measures clearly show results comparable to the ones observable for the usage of purely color-based descriptors, with improvements for classes like beach that tend otherwise to be confused with the colorimetrically similar yet geometrically separate building roofs.

For the construction of a test site set, we consider five different geographical areas in the Basque country with different kinds of surfaces, as per Fig. 6. The selected areas represent a coastal bay (the La Concha beach area), a highlands area, an industrial area in the outskirts of the city of Bilbao, an urban area in the city of Vitoria Gasteiz, and a site in the protected natural area of Urdaibai, geographically located in correspondence to the red points in the map in Fig. 5.

The obtained classification result is shown in Fig. 6(c).

C. Local Classifier Evaluation Based on Both Semiautomatically Generated, Vector Map-Derived, and Manually Curated, Pixel-Level, Image Interpretation-Based Ground Truths

As described in Section IV-A, we complement the evaluation of the supervised classification system with respect to a five-site map-based ground truth with a more localized pixel-level ground truth obtained by manual interpretation of the image content.

Because of the difficulty of developing a pixel level ground truth of all areas, the analysis has been limited to one site of the five considered in previous sections. Among the five sites, we consider the La Concha bay site since it is the most complex with eight ground coverage classes: 1) beach; 2) buildings;

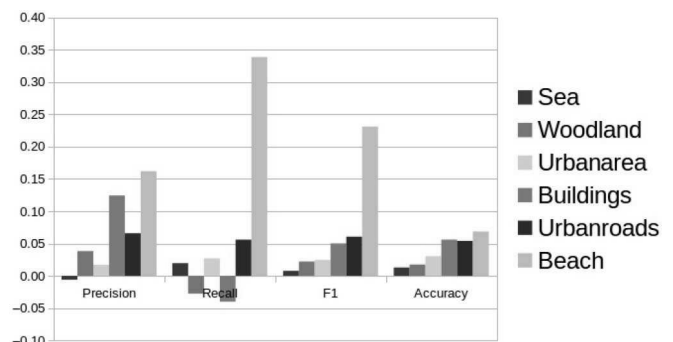


Fig. 10. Difference of quality measures by class for a classification based on color descriptors exclusively and on full set of descriptors. The results are similar, with marked improvements for homogeneous classes like beach, and a significant decrease for buildings, characterized by a very large internal variability that typically is not accounted for by the training.

3) bare soil; 4) pasture; 5) woodland; 6) roads; 7) sea; and 8) urban area.

The obtained results are shown in Table VI and Fig. 11.

Performance measures obtained with reference to the image interpretation-based ground truth tend to show improvements between 20% and 60% with respect to the ones obtained with reference to the map-based ground truth, because of both the availability of details that are not available in the maps and of the fact that the time of reference considered matches the image acquisition time, which is important in the case of rapidly changing sites such as the Urdaibai estuary. Class pasture is an example of this, where city gardens and other trees groups are not identified on shape base ground truth. Urban area and urban road classes present a decrement of precision related to the increment of false positive cases related to the different tagging in the two ground-truth maps, see top right corner of center and right images in Fig. 8.

Thematic map generation by the system requires about one minute for the whole 28 MPixel image considered on a 2.0-GHz Intel TM I7 4750HQ with 8 GB of RAM and SSD disk equipping a laptop computer.

TABLE VI
PERFORMANCE MEASURES FOR THE LA CONCHA BAY SITE WITH RESPECT TO THE MANUALLY CURATED PIXEL-LEVEL IMAGE
INTERPRETATION-BASED GROUND TRUTH

Performance	Sea		Woodland		Bare soil		Urban area		Pasture		Buildings		Urban roads		Beach	
statistics	Vector	Pixel	Vector	Pixel	Vector	Pixel	Vector	Pixel	Vector	Pixel	Vector	Pixel	Vector	Pixel	Vector	Pixel
Precision	0.99	0.99	0.28	0.48	0.00	0.06	0.37	0.22	0.00	0.55	0.52	0.66	0.03	0.16	0.69	0.73
Recall	0.90	0.87	0.34	0.48	0.00	0.08	0.15	0.14	0.00	0.07	0.29	0.30	0.05	0.30	0.77	0.92
F1	0.94	0.93	0.31	0.48	0.00	0.07	0.22	0.17	0.00	0.13	0.37	0.41	0.04	0.21	0.73	0.81
Accuracy	0.91	0.90	0.89	0.91	0.96	0.95	0.84	0.87	0.99	0.94	0.91	0.91	0.89	0.92	0.91	0.94

These results are obtained by only considering the La Concha Bay Test Site, hence the number of ground cover classes is reduced from the original 12 to only 8.

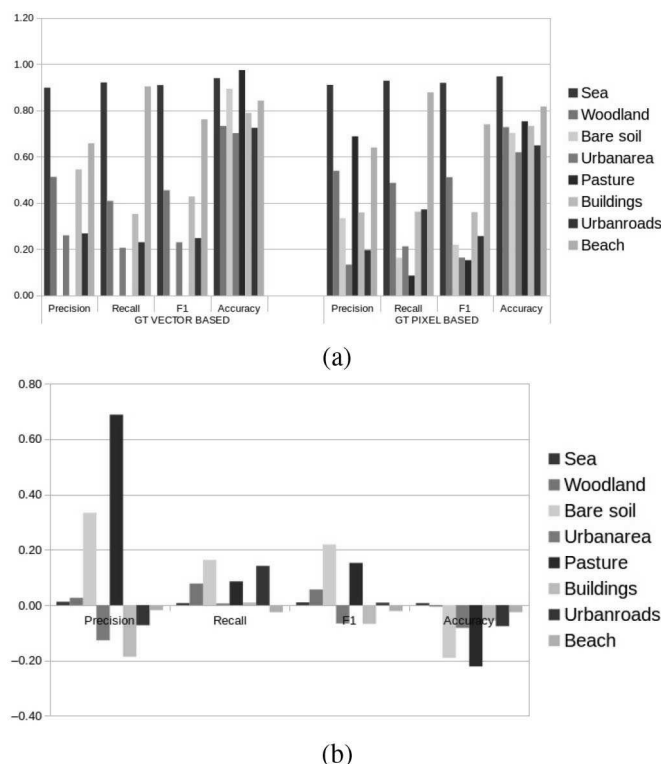


Fig. 11. Quality measures by ground cover class for a supervised classification with respect to two different ground-truth maps (existing vector map-based on the left, and manually produced pixel-level image interpretation based on the right) (a) and the difference of obtained results (b). These results are obtained by only considering the La Concha bay test site, hence the number of ground cover classes is reduced from the original 12 to only 8. Although they cannot be directly extrapolated to the full test site set, they indicate that the lack of spatial detail and the choice of a different temporal reference with respect to image acquisition can account for a 20 to 60% of difference in the obtained performance measures. Ground cover class Pasture is an example of this: gardens and small trees groups are not identified in the map-based ground truth.

VI. CONCLUSION

We have presented a prototype for thematic mapping from remote-sensing raster data.

The prototype is based on a probabilistic k-nearest neighbor supervised classification algorithm integrated in a simple Web-based architecture, and attains fast processing performance by exploiting N-dimensional data indexing structures, with the final aim of allowing users to interactively navigate and semantically map large extensions of geospatial data.

Results are promising for submetric airborne optical sensor data. The enrichment of the ground truth with the onset of

new classes and improvement on performance measures validated pixel-based ground-truth creation. Implementations on top of “big data” cluster computing framework will need to be considered to further enhance scalability.

REFERENCES

- [1] M. Quartulli and I. G. Olaizola, “A review of EO image information mining,” *ISPRS J. Photogramm. Remote Sens.*, vol. 75, pp. 11–28, Jan. 2013 [Online]. Available: <http://linkinghub.elsevier.com/retrieve/pii/S0924271612001797>
- [2] M. Koubarakis *et al.*, “Building virtual earth observatories using ontologies, linked geospatial data and knowledge discovery algorithms,” in *On the Move to Meaningful Internet Systems: OTM 2012*, R. Meersman *et al.*, Eds. New York, NY, USA: Springer, 2012, vol. 7566, pp. 932–949.
- [3] M. Schröder, H. Rehrauer, K. Seidel, and M. Datcu, “Interactive learning and probabilistic retrieval in remote sensing image archives,” *IEEE Trans. Geosci. Remote Sens.*, vol. 38, no. 5, pp. 2288–2298, Sep. 2000.
- [4] H. Costa, H. Carrão, F. Baçao, and M. Caetano, “Combining per-pixel and object-based classifications for mapping land cover over large areas,” *Int. J. Remote Sens.*, vol. 35, no. 2, pp. 738–753, 2014.
- [5] S. W. Myint, P. Gober, A. Brazel, S. Grossman-Clarke, and Q. Weng, “Per-pixel vs. object-based classification of urban land cover extraction using high spatial resolution imagery,” *Remote Sens. Environ.*, vol. 115, no. 5, pp. 1145–1161, 2011.
- [6] U. Maulik and A. Sarkar, “Efficient parallel algorithm for pixel classification in remote sensing imagery,” *Geoinformatica*, vol. 16, no. 2, pp. 391–407, 2012.
- [7] Q. Ho, P. Lundblad, T. Aström, and M. Jern, “A web-enabled visualization toolkit for geovisual analytics,” *Inf. Vis.*, vol. 11, no. 1, pp. 22–42, 2012.
- [8] P. Keel, “Collaborative visual analytics: Inferring from the spatial organization and collaborative use of information,” in *Proc. IEEE Symp. Visual Anal. Sci. Technol.*, Oct. 2006, pp. 137–144.
- [9] A. Ferran, S. Bernabe, P. G. Rodríguez, and A. Plaza, “A web-based system for classification of remote sensing data,” *IEEE J. Sel. Topics Appl. Earth Observ. Remote Sens.*, vol. 6, no. 4, pp. 1934–1948, Aug. 2013.
- [10] R. Cheng, L. Chen, J. Chen, and X. Xie, “Evaluating probability threshold k-nearest-neighbor queries over uncertain data,” in *Proc. 12th Int. Conf. Extending Database Technol. Adv. Database Technol.*, 2009, pp. 672–683.
- [11] S. Maneewongvatana and D. M. Mount, “On the efficiency of nearest neighbor searching with data clustered in lower dimensions,” in *Proc. Int. Conf. Comput. Sci. I*, vol. 2073, V. N. Alexandrov, J. Dongarra, B. A. Julian, R. S. Renner, and C. J. K. Tan, Eds. New York, NY, USA: Springer, 2001, pp. 842–851.
- [12] M. Datcu *et al.*, “Information mining in remote sensing image archives: System concepts,” *IEEE Trans. Geosci. Remote Sens.*, vol. 41, no. 12, pp. 2923–2936, Dec. 2003.
- [13] A. W. Smeulders, M. Worring, S. Santini, A. Gupta, and R. Jain, “Content-based image retrieval at the end of the early years,” *IEEE Trans. Pattern Anal. Mach. Intell.*, vol. 22, no. 12, pp. 1349–1380, Dec. 2000.
- [14] R. Datta, D. Joshi, J. Li, and J. Z. Wang, “Image retrieval: Ideas, influences, and trends of the new age,” *ACM Comput. Surv.*, vol. 40, no. 2, pp. 5:1–5:60, May 2008.
- [15] J. M. Peña-Barragán, M. K. Ngugi, R. E. Plant, and J. Six, “Object-based crop identification using multiple vegetation indices, textural features and crop phenology,” *Remote Sens. Environ.*, vol. 115, no. 6, pp. 1301–1316, 2011.

- [16] M. Blume and D. R. Ballard, "Image annotation based on learning vector quantization and localized haar wavelet transform features," *Proc. SPIE* vol. 3077, pp. 181–190, 1997.
- [17] I. G. Olaizola, M. Quartulli, J. Florez, and B. Sierra, "Trace transform based method for color image domain identification," *IEEE Trans. Multimedia*, vol. 16, no. 3, pp. 679–685, Apr. 2014.
- [18] I. G. Olaizola, G. Marcos, P. Kramer, J. Florez, and B. Sierra, "Architecture for semi-automatic multimedia analysis by hypothesis reinforcement," in *Proc. IEEE Int. Symp. Broadband Multimedia Syst. Broadcast. (BMSB'09)*, 2009, pp. 1–6.
- [19] N. Chauffert, J. Israel, and B. Le Saux, "Boosting for interactive man-made structure classification," in *Proc. IEEE Int. Geosci. Remote Sens. Symp. (IGARSS'12)*, 2012, pp. 6856–6859.
- [20] R. Spiekermann, M. Brandt, and C. Samimi, "Woody vegetation and land cover changes in the Sahel of Mali (1967–2011)," *Int. J. Appl. Earth Observ. Geoinf.*, vol. 34, pp. 113–121, 2015 [Online]. Available: <http://www.sciencedirect.com/science/article/pii/S0303243414001718>
- [21] E. Li, J. Femiani, S. Xu, X. Zhang, and P. Wonka, "Robust rooftop extraction from visible band images using higher order CRF," *IEEE Trans. Geosci. Remote Sens.*, vol. 53, no. 8, pp. 4483–4495, Aug. 2015.
- [22] J. Han, D. Zhang, G. Cheng, L. Guo, and J. Ren, "Object detection in optical remote sensing images based on weakly supervised learning and high-level feature learning," *IEEE Trans. Geosci. Remote Sens.*, vol. 53, no. 6, pp. 3325–3337, Jun. 2015.
- [23] W. Yang, X. Yin, and G. Xia, "Learning high-level features for satellite image classification with limited labeled samples," *IEEE Trans. Geosci. Remote Sens.*, vol. 53, no. 8, pp. 4472–4482, Aug. 2015 [Online]. Available: <http://dx.doi.org/10.1109/TGRS.2015.2400449>
- [24] A. Cheriadat, "Unsupervised feature learning for aerial scene classification," *IEEE Trans. Geosci. Remote Sens.*, vol. 52, no. 1, pp. 439–451, Jan. 2014.
- [25] Y. Yang and S. Newsam, "Geographic image retrieval using local invariant features," *IEEE Trans. Geosci. Remote Sens.*, vol. 51, no. 2, pp. 818–832, Feb. 2013.
- [26] C. Pohl and J. Van Genderen, "Review article multisensor image fusion in remote sensing: Concepts, methods and applications," *Int. J. Remote Sens.*, vol. 19, no. 5, pp. 823–854, 1998.
- [27] M. Molinier, J. Laaksonen, and T. Hame, "Detecting man-made structures and changes in satellite imagery with a content-based information retrieval system built on self-organizing maps," *IEEE Trans. Geosci. Remote Sens.*, vol. 45, no. 4, pp. 861–874, Apr. 2007.
- [28] J. Inglada and E. Christophe, "The Orfeo toolbox remote sensing image processing software," in *Proc. IEEE Int. Geosci. Remote Sens. Symp. (IGARSS'09)*, 2009, pp. 733–736.
- [29] X. Perrotton, M. Sturzel, and M. Roux, "Automatic object detection on aerial images using local descriptors and image synthesis," in *Computer Vision Systems*. New York, NY, USA: Springer, 2008, pp. 302–311.
- [30] J. Lozano, M. Quartulli, I. Tamayo, M. Laka, and I. G. Olaizola, "Visual analytics for built-up area understanding from metric resolution earth observation data," *ISPRS Int. Arch. Photogramm. Remote Sens. Spatial Inf. Sci.*, vol. XL7/W2, pp. 151–154, 2013.
- [31] J. Lozano, N. Aginako, M. Quartulli, and I. G. Olaizola, "Semi automatic remote sensing image layer generator based on web based visual analytics," in *Proc. 5th Jubilee Int. Conf. Cartography GIS*, 2014, pp. 709–714.
- [32] C. D. Manning, P. Raghavan, and H. Schütze, *Introduction to Information Retrieval*. Cambridge, U.K.: Cambridge Univ. Press, 2008.



of the Basque Country (UPV/EHU) University, Vizcaya, Spain. He is currently pursuing the Ph.D. degree in system engineering and automation at the University of the Basque Country, Bilbao, Spain.

Afterward, he developed the End of Degree Project in Orona EIC S.COOP about "The Enhancement of the Functionalities of Teleservicio, in 2005". Since February 2008, he has been working with Vicomtech-Ik4 Research Center (www.vicomtech.org), Donostia, Spain.



Naiara Aginako Bengoa received the Telecommunications Engineering degree from the University of the Basque Country, Vizcaya, Spain, in 2005. Currently, she is pursuing the Ph.D. degree in image analysis and content-based retrieval of images and video at the University of the Basque Country, San Sebastián, Spain.

From 2003 to 2005, she collaborated the Signal Processing and Communication Group, Electronics and Telecommunications Department with the University of the Basque Country, EHU/UPV, San Sebastián, Spain. She develops and manages research projects in Vicomtech-IK4, Donostia, Spain, since 2005, in the Digital Media Department. She is also a teacher with the Politechnique School of Donostia, Donostia, Spain, for more than 3 years. Her work as a Researcher counts on a number of publications and on two patents Biography text here.



Marco Quartulli (SM'03) received the Laurea degree in physics from the University of Bari, Bari, Italy, in 1997, and the Ph.D. degree in electrical engineering and computer science from the University of Siegen, Siegen, Germany, in 2005.

From 1997 to 2010, he worked on remote-sensing ground segment engineering, image analysis, archives, and mining with the Advanced Computer Systems, Rome, Italy. From 2000 to 2003, he was with the Image Analysis Group, Remote Sensing Technology Institute, German Aerospace Center (DLR), Cologne, Germany, working on metric resolution synthetic aperture radar image understanding in urban environments and content-based image retrieval. Since 2010, he has joined the Multimedia Services Department, Vicomtech-IK4, Donostia, Spain, where he is working on large-scale analytics for the multimedia and the geospatial analysis domains.



Igor G. Olaizola (SM'14) received the Degree in electronic and control engineering from the University of Navarra, Navarra, Spain, in 2001, and the Ph.D. degree in informatics from the Faculty of Informatics of San Sebastián, University of the Basque Country, Vizcaya, Spain, in 2014.

He developed his master thesis at Fraunhofer Institut für Integrierte Schaltungen (IIS), Erlangen, Germany, in 2001, where he worked for a year as Research Assistant on several projects related to MPEG standard audio decoding. Currently, he is the Head of the Digital Interactive TV and Multimedia Services Department. In 2006, he was a Technology Consultant for 1 year with Vilau Company, Zamudio, Spain.

Dr. Olaizola has been a member of Vicomtech Technological Centre since 2002.



Ekaitz Zulueta received the B.S. degree in electronic engineering from Mondragon University, Arrasate, Spain, in 1997, and the M.S. degree in electrical engineering from Swiss Institute of Technology Lausanne, Lausanne, Switzerland, in 2000, and the Ph.D. degree in control engineering from the University of the Basque Country, Vizcaya, Spain, in 2005.

From 2000 to 2002, he has been employed as a Research Engineer with Ideko, Elgoibar, Spain and Fagor Automation, Arrasate-Mondragon, Spain. Since 2002, he has been employed as a Lecturer with the University of the Basque Country (University College of Engineering of Vitoria-Gasteiz), Vizcaya, Spain. His research interests cover a range of computational intelligence areas including image processing and wind turbines control.